Available online at www.sciencedirect.com

SciVerse ScienceDirect

Journal of the European Ceramic Society 32 (2012) 865–873

www.elsevier.com/locate/jeurceramsoc

Effect of TiO_2 doped Ni electrodes on the dielectric properties and microstructures of $(Ba_{0.96}Ca_{0.04})(Ti_{0.85}Zr_{0.15})O_3$ multilayer ceramic capacitors

Chen-Su Chiang [a], Ying-Chieh Lee [b,*], Fu-Thang Shiao [c], Wen-Hsi Lee [a], Detlev Hennings [d]

[a] *Department of Electrical Engineering, National Cheng Kung University, Tainan 701, Taiwan*
[b] *Department of Material Engineering, National Pingtung University of Science & Technology, Pingtung, Taiwan*
[c] *Department of Material Research, Walsin Technology Corporation, Kaohsiung, Taiwan*
[d] *Department of Electronic Materials, Forschungszentrum Jülich GmbH, Jülich D-52425, Germany*

Received 26 September 2011; received in revised form 2 November 2011; accepted 6 November 2011
Available online 30 November 2011

Abstract

The effects of TiO_2-doped Ni electrodes on the microstructures and dielectric properties of $(Ba_{0.96}Ca_{0.04})(Ti_{0.85}Zr_{0.15})O_3$ multilayer ceramic capacitors (MLCCs) have been investigated. Nickel paste with a TiO_2 dopant was used as internal electrodes in MLCCs based on $(Ba_{0.96}Ca_{0.04})(Ti_{0.85}Zr_{0.15})O_3$ (BCTZ) ceramic with copper end-termination. The microstructures and defects were analysed by microstructural techniques (SEM/HRTEM) and energy-dispersive spectroscopy (EDS). The continuity of the electrode of the MLCC was measured using a scanning electron microscope, which showed that the continuity of the electrode for the MLCC with a TiO_2-doped Ni electrode was approximately 90%. However, continuity of the electrode for a conventional MLCC was below 80%. The continuity of the TiO_2-doped Ni electrode showed significant improvement in the MLCC, which was due to no reaction between Ni and BCTZ.

Keywords: TiO_2 doped Ni electrode; MLCC; Reducing atmosphere; $(Ba_{0.96}Ca_{0.04})(Ti_{0.85}Zr_{0.15})O_3$

1. Introduction

Barium titanate ($BaTiO_3$, BT), a perovskite structure, has been widely investigated because of its dielectric and ferroelectric properties.[1,2] Materials with high dielectric constants, such as $(Ba,Ca)(Ti,Zr)O_3$ ceramics, are commonly applied as key materials for high capacitance multilayer ceramic capacitors (MLCCs) with an application specification of Y5V. MLCCs exhibit broad dielectric maxima (ε_{max}) and can have peak values of up to $\varepsilon_{max} \approx 18{,}000$ when prepared in oxidising atmospheres.[3] Ca and Zr are employed to broaden the dielectric maximum at the Curie point and to shift it to room temperature, respectively. Replacing the precious metal with a more common metal in an MLCC can significantly reduce production costs. One of the best candidates for such a replacement is Ni. In this case, the dielectric should be co-fired in a reducing atmosphere to prevent the oxidation of the internal electrode.

Dielectric formulation and process technology for MLCC has been extensively investigated in the electronics industry.[4–6] The sintering process and the ceramic composition are considered to be the two key factors leading to the unwanted failures, etc. resistance degradation and breakdown. Great effort has been devoted to optimizing the sintering process and adjusting the ceramic composition.[7–10] More attention must be given to the sintering process to control the shrinkage mismatch between the dielectric and electrode layers in MLCCs, as this is the main reason for residual stress resulting in cracking and delamination during fabrication and service.[11–14] Usually, there are two ways of reducing the shrinkage mismatch between the dielectric and electrode layers in MLCCs, the first is the addition of a dielectric material into the Ni paste to postpone the shrinkage of Ni electrodes during firing, and the second is to decrease the firing temperature of the dielectric material by adding sintering aids to control the shrinkage mismatch.[15–17] The addition of a sintering aid such as glass to $BaTiO_3$ is an effective method

* Corresponding author. Tel.: +886 8 7703202; fax: +886 8 7740552.
E-mail address: YCLee@mail.npust.edu.tw (Y.-C. Lee).

0955-2219/$ – see front matter.
doi:10.1016/j.jeurceramsoc.2011.11.009

which increases the density of the dielectric ceramics at low temperatures. Anyway, numerous kinds of glasses have been developed as sintering aids for $BaTiO_3$.[18–23] The addition of a dielectric material to the Ni paste is an effective method which reduces the shrinkage of Ni electrodes (increases the continuity of Ni electrodes) during firing, but it will lower the conductivity of electrodes when too much dielectric material is added to the Ni paste.

Titanium dioxide occurs in nature as the well-known minerals rutile, anatase and brookite. The most common form is rutile,[24] which is also the stable equilibrium phase at all temperatures.[25] Rutile contains six-coordinated titanium with a high melting point of ~1843 °C, which is higher than the melting point of $BaTiO_3$ (1625 °C).

In this paper, we investigated the effects of TiO_2 doped Ni electrodes on the sintering behaviour, the dielectric properties, and the microstructural of BCTZ MLCC. Moreover, the interfacial reaction between BCTZ and TiO_2 doped Ni electrodes was also studied.

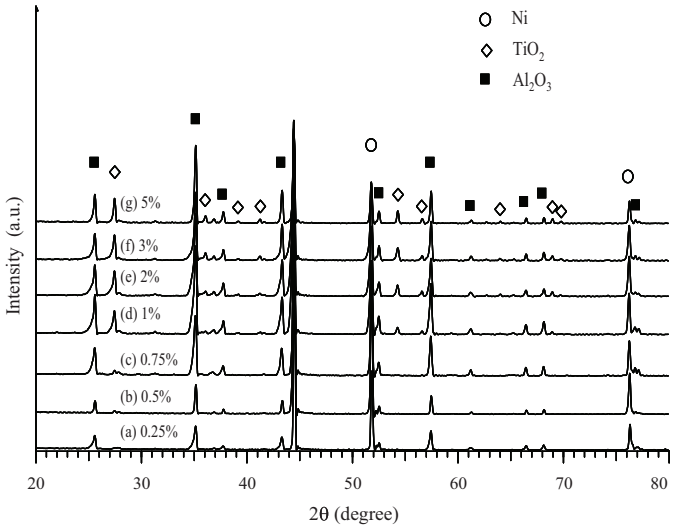

Fig. 1. X-ray diffraction (XRD) spectra of Ni paste printed on an Al_2O_3 substrate, which was sintered at 1220 °C and doped with different amounts of TiO_2.

2. Experimental procedures

2.1. Preparation of the BCTZ powders

Conventional ceramic fabrication processes were used to prepare the $(Ba_{0.96}Ca_{0.04})(Ti_{0.85}Zr_{0.15})O_3$ (BCTZ) samples using commercial powders of $BaCO_3$, $CaCO_3$, ZrO_2 and TiO_2. The BCTZ samples were doped with 0.03 mol.% Mn acceptor and 0.15 mol.% SiO_2 sintering aid in this study. The $BaCO_3$, $CaCO_3$, ZrO_2, TiO_2, MnO_2 and SiO_2 powders were mixed with deionized water for 24 h in a ϕ 2 mm zirconia ball-mill. The mixture was dried, calcined at 1150 °C for 6 h in air, and then crushed into powder.

2.2. Nickel paste preparation

TiO_2-doped Ni pastes were prepared using various amounts of titania (e.g., 0.25, 0.5, 1, 2, and 3 wt.% titania content). TiO_2 powder (F2-A, 99.08% purity) was as supplied by Showa Titanium Co., Ltd., Japan. The particle size was approximately 0.2 μm and surface area was about 10 m^2/g. Nickel powder (99.0%, median particle size is 0.3 μm) was made by Wako Pure Chemical Ind., Japan. The paste properties consist of 50% solid content and 50 Pa-s of viscosity at 10 rpm. The paste was rolled several times using a three roll mill. To measure the shrinkage rate and electrical resistivity of TiO_2-doped Ni paste after sintering, the TiO_2-doped Ni paste was printed onto a Al_2O_3 substrate

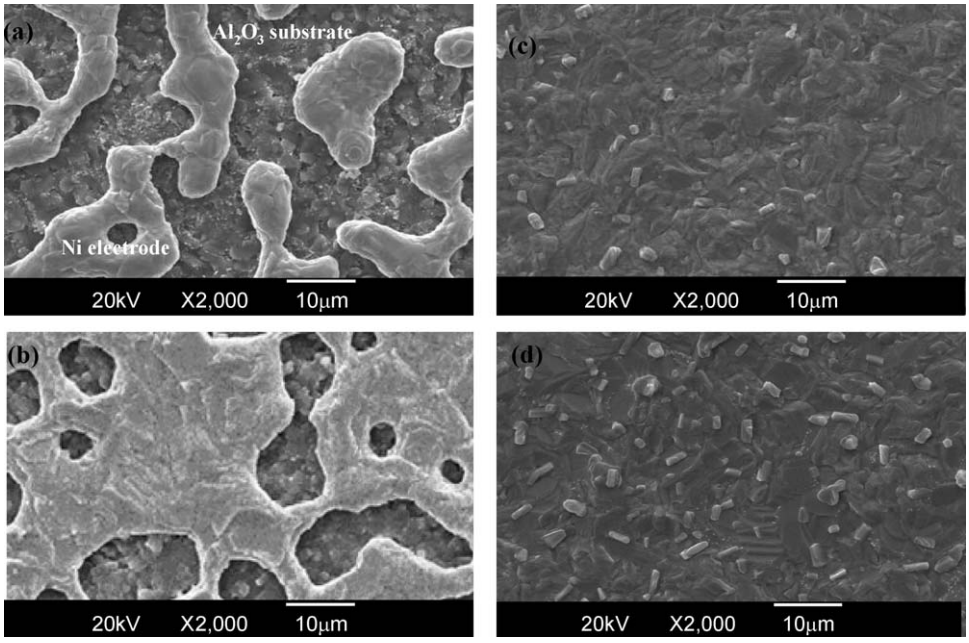

Fig. 2. Scanning electron microscopic micrographs of the Ni paste printed on Al_2O_3 substrates and sintered at 1220 °C with (a) 0 wt.%, (b) 0.5 wt.%, (c) 1 wt.%, and (d) 2 wt.% TiO_2 added.

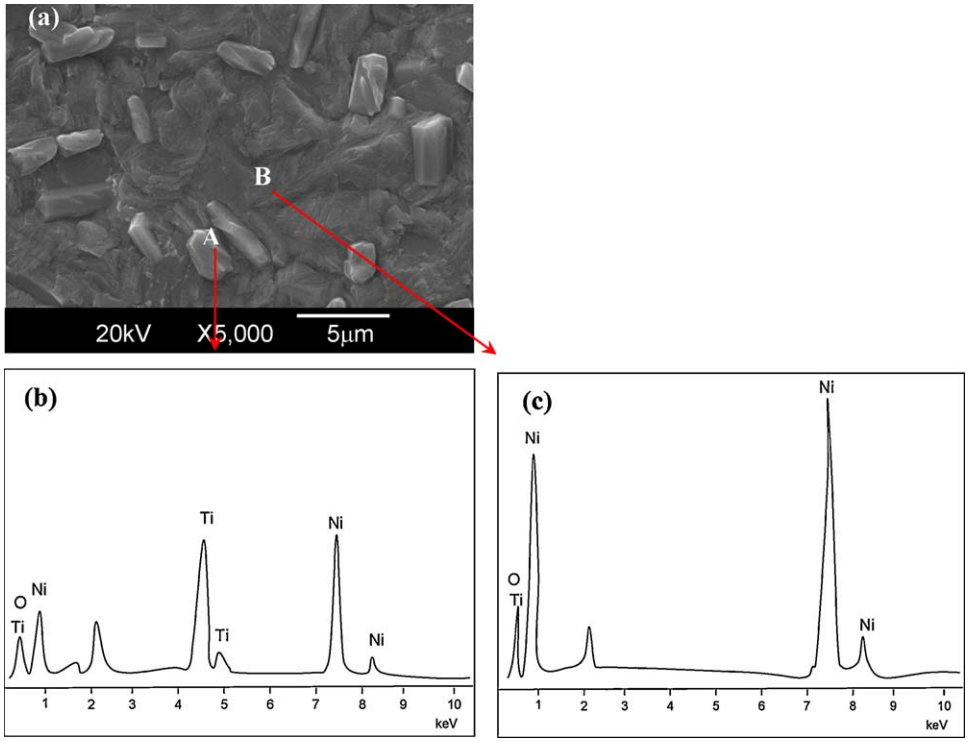

Fig. 3. The (a) microstructure micrographs, (b) EDS for the A position, and (c) EDS for the B position for the 3 wt.% TiO_2-doped Ni paste printed on an Al_2O_3 substrate sintered at 1220 °C.

and sintered at 1220 °C for 2 h in a reducing atmosphere (at an oxygen partial pressure $< 10^{-10}$ Pa). The electrical resistivity of samples was determined by the four-point probe technique.

2.3. Fabrication of multilayered BCTZ capacitors

The BCTZ powders were mixed with resin (polyvinyl butyral), plasticiser (butyl benzyl phthalate), and solvent (toluene and ethanol). The resultant slurry was tape-casted to a green sheet with a 30 μm thickness using the doctor-blade method. TiO_2-doped Ni paste was printed as an internal electrode onto the green sheet. These printed sheets were stacked, pressed at 60 °C under a pressure of 5.2×10^7 Pa, and cut into chips. The laminated green chips were sintered at 1220 °C for 2 h in a reducing atmosphere (oxygen partial pressure $< 10^{-10}$ Pa). After the binder burns out (320 °C), the sintered chip is then called a brick. Subsequently, annealing in an oxygen partial pressure below 1.7×10^{-6} Pa at 1000 °C was carried out to reoxidise the ceramic bodies.

2.4. Analysis and measurement

The density of the sintered composites was measured using the Archimedes method. The microstructures of polished samples were examined by scanning electron microscopy (SEM, model S2500, Hitachi, Tokyo, Japan). The mean grain size was calculated using the line intercept method. Copper electrodes were attached to the sintered bricks and fired at 900 °C for 10 min to measure its electrical properties. The dielectric permittivity and the dissipation factor of the MLCCs were measured using an impedance analyzer (Agilent Technology HP4284A). The measurement was carried out over the temperature range of −30 °C to 85 °C at 1 Vrms. The insulation resistance (IR) was measured using a high resistance meter (Agilent Technology HP4339B) at room temperature. Microstructures of samples were investigated by filed-emission transmission electron microscopy (FE-TEM, FEI E.O. Tecnai F20) at an acceleration voltage of 200 kV, equipped with energy-dispersive spectroscopy (EDS).

3. Results and discussion

3.1. Characteristic evaluation for TiO_2 doped Ni thick films

The influence of TiO_2-doped Ni electrodes on the microstructural characteristics and dielectric properties of BCTZ MLCCs

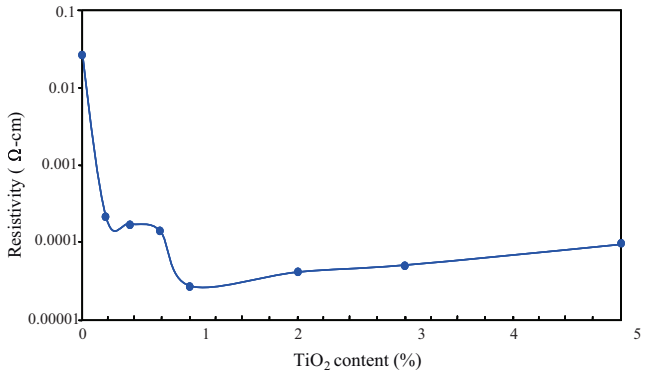

Fig. 4. The electrical resistivity of Ni paste sintered at 1220 °C as a function of the amount of TiO_2 added.

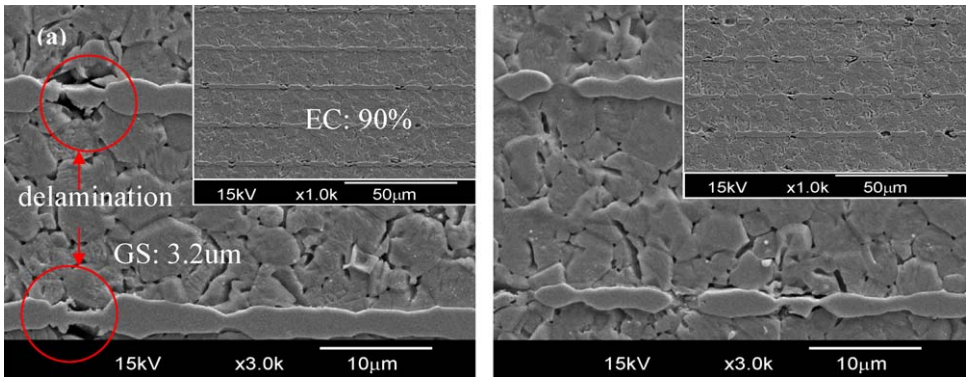

Fig. 5. Microstructure micrographs of the BCTZ MLCCs sintered at 1220 °C with (a) 1 wt.% TiO_2 and (b) 3 wt.% TiO_2-doped Ni electrodes.

were studied in this report. The interaction of TiO_2 with the Ni electrode after firing was investigated using X-ray diffraction. Fig. 1 shows the XRD patterns of the Ni electrodes with different TiO_2 additions after being sintered at 1220 °C for 2 h in a reducing atmosphere. The TiO_2 peaks were enhanced with increasing amounts of TiO_2 added to Ni, which indicates that there is no interaction between TiO_2 and Ni during high temperature sintering. Fig. 2 shows the SEM images of Ni pastes sintered at 1220 °C with TiO_2 concentrations of 0, 0.5, 1, and 2 wt.%. High levels of shrinkage were observed for the samples without TiO_2, as shown in Fig. 2(a). When TiO_2 was added to the Ni paste, the shrinkage of thick Ni films significantly decreased, as shown in Fig. 2(b)–(d). The addition of TiO_2 retards the shrinkage of the thick Ni films, which leads to better interfacial matching between the Ni film and the Al_2O_3 substrate. Energy dispersive spectroscopy (EDS) was used to identify the secondary

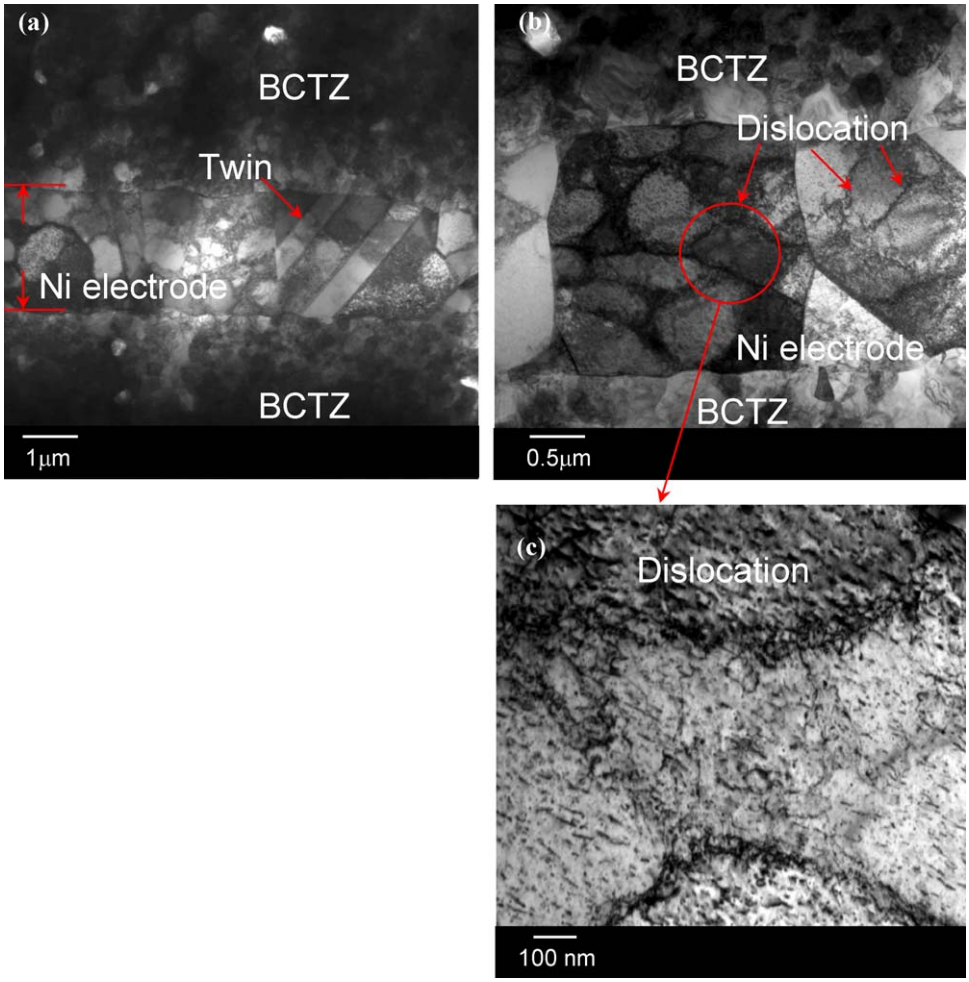

Fig. 6. HRTEM micrographs of the BCTZ MLCC sintered at 1220 °C with a 3 wt.% TiO_2-doped Ni electrode showing (a) the BCTZ dielectric and Ni electrode, and (b and c) their dislocations.

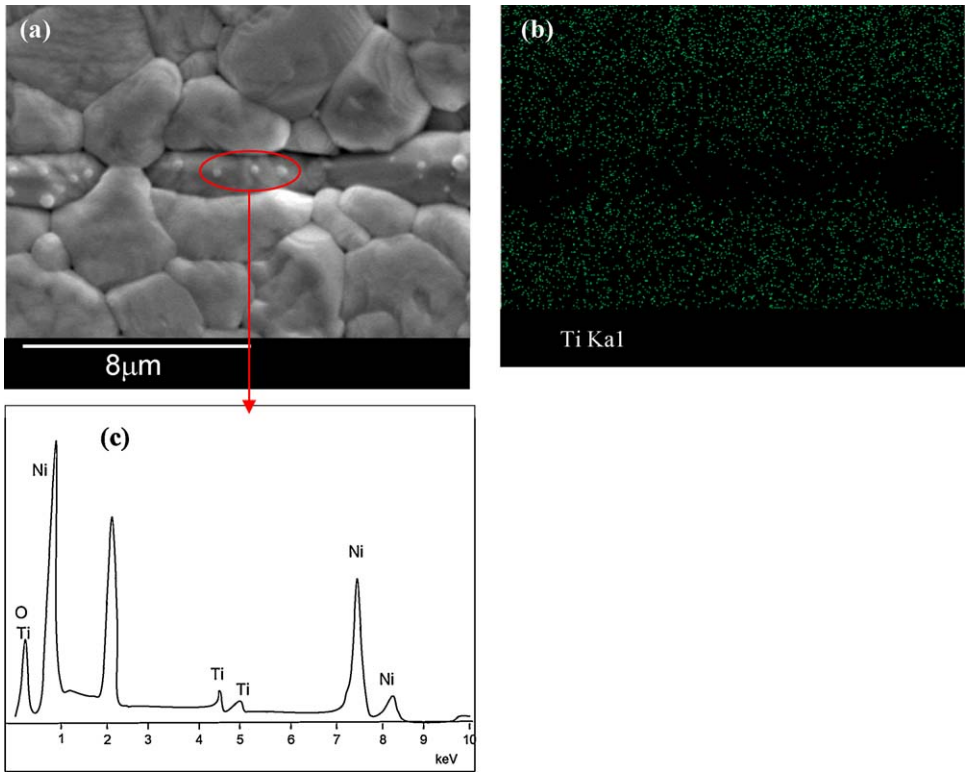

Fig. 7. MLCCs with a 3 wt.% TiO_2-doped Ni electrode sintered at 1220 °C with (a) microstructure micrographs, (b) the Ti elemental mapping, and (c) the EDS spectrum of the Ni electrode part.

phases. The microstructure micrographs of 3 wt.% TiO_2-doped Ni paste sintered at 1220 °C are shown in Fig. 3. Compared with matrix phase "B" (Fig. 3(c)), the strip-like grains of "A" have higher signal intensities in Ti (Fig. 3(b)). According to the X-ray diffraction analysis in the previous section, it clearly shows that the existence of the TiO_2 phase at $TiO_2 \geq 1$ wt.%. It is therefore believed that the strip-like grains are composed of TiO_2. Fig. 4 shows the resistivity of the Ni pastes sintered at 1220 °C as a function of TiO_2 concentrations. The resistivity significantly decreased with the addition of TiO_2. The resistivities of the thick films were 5×10^{-2}, 3×10^{-4}, 2×10^{-4}, 1×10^{-4}, and 4×10^{-5} Ω-cm for 0, 0.25, 0.5, 0.75, and 1 wt.% TiO_2 dopant, respectively. The reason the pure nickel film had a higher resistivity was due to high shrinkage after sintering, as shown in Fig. 2. It is known that the degree of densification is important in determining the electrical behaviour of thick films.[14–16]

3.2. *Effect of TiO_2 doped Ni electrodes on the microstructures of BCTZ MLCC*

A green sheet was prepared by tape casting using the BCTZ powders. TiO_2-doped Ni paste was attached to the green sheet as an internal electrode. After lamination, the green chips were sintered at 1220 °C for 2 h, and the external Cu electrodes were attached as the terminations. To understand the electrode continuity of the TiO_2-doped Ni paste and microstructures of the ZMT dielectrics in the MLCC, a cross-sectional of the MLCC was prepared as shown in Fig. 5. The microstructure of MLCC with 1 wt.% TiO_2-doped Ni electrodes was analysed as shown in Fig. 5(a). It can be seen that the continuity of the internal electrodes in the MLCC was approximately 90% with a laydown of approximately 0.7 mg/cm^2. The dielectric film thickness after sintering was approximately 17 μm, and the electrode thickness was approximately 2.4 μm. Fig. 5(b) shows the microstructure of the MLCC with 3 wt.% TiO_2-doped Ni electrodes, the continuity of the internal electrodes in the MLCC was approximately 84% with a laydown of approximately 0.7 mg/cm^2. The results indicate that the continuity of the internal electrode decreased as the amount of TiO_2 in the Ni paste increased. The continuity of the internal electrode could be regarded as the TiO_2 content of the internal electrode of the MLCC. This may be due to a high presence of TiO_2 in the internal electrodes, as shown in Figs. 1 and 2, which will reduce the continuity of electrodes when additional ceramic materials are added to the Ni paste. The continuity of the internal electrodes in commercial MLCCs is generally below 80%, particularly with reference to the Y5V-1206 MLCCs rated 1 μF.[17] Pure $BaTiO_3$ powders are often added to the metal inner electrodes to decrease the coefficient mismatch of thermal expansion and increase the sintering match with the dielectric layers. Most importantly, interfacial reactions may occur between the internal TiO_2-doped Ni electrode and the dielectric ceramic layer. There is a good physical match between 3 wt.% TiO_2-doped Ni electrodes (Fig. 5(b)) and BCTZ dielectrics resulting from inferior interfacial bonding; however, some delamination in the MLCC with 1 wt.% TiO_2-doped Ni electrodes was observed, as shown in Fig. 5 (a). The grain size of MLCCs with 1 and 3 wt.% TiO_2-doped Ni internal electrodes is

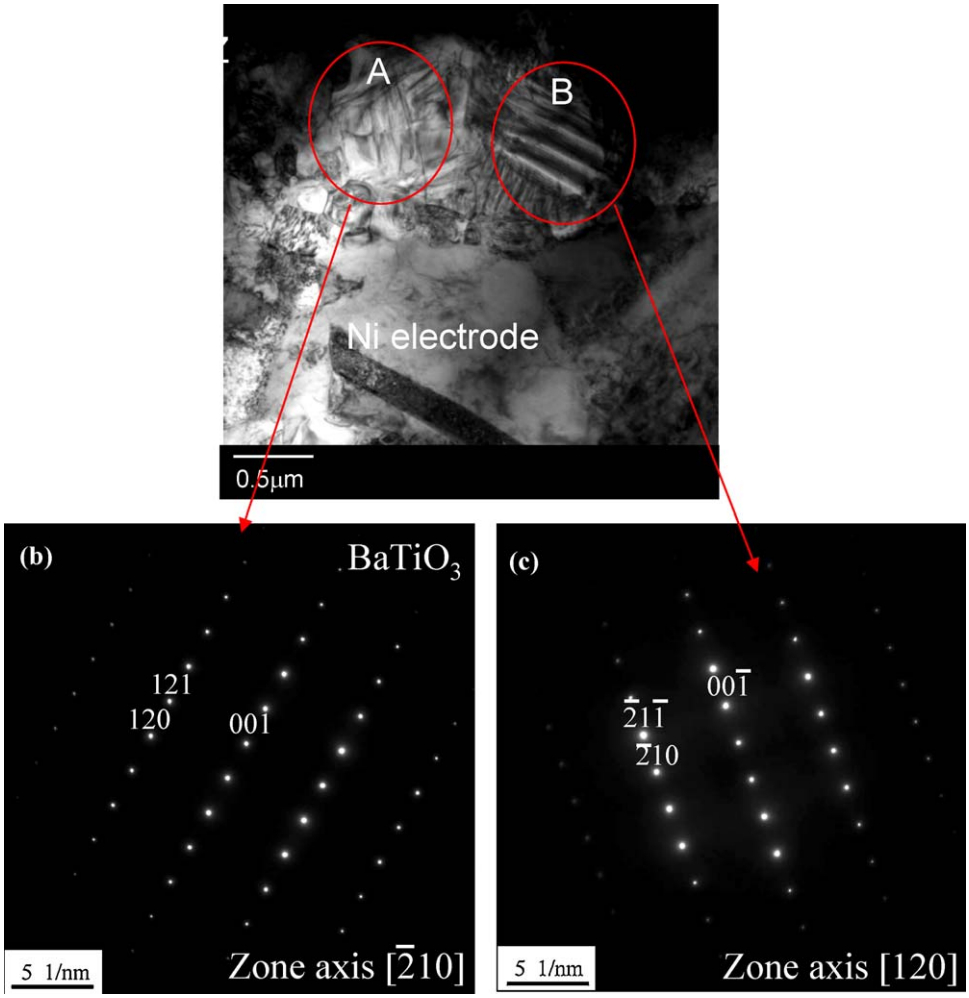

Fig. 8. HRTEM micrographs of the BCTZ MLCC sintered at 1220 °C with a 3 wt.% TiO_2-doped Ni electrode showing (a) the normal grain and twins of BCTZ, (b) the SAD of BCTZ normal grain, and (c) the SAD of BCTZ twin grain.

3.2 μm and 3.9 μm, respectively. This result indicates that some of the TiO_2 dopant in the Ni electrode leads to slight grain growth of the BCTZ dielectrics. This may be attributed to small changes in the *A*/*B* ratio of BCTZ dielectrics during sintering because Ti ions will diffuse into the dielectric layer from TiO_2-doped Ni electrodes during firing. Lee et al.[26] have reported that the grain size is significantly influenced by changes in the *A*/*B* ratio in the BCTZ material system. When the *A*/*B* ratio was decreased, the average grain size of the samples increased, which enhanced grain growth. High-resolution transmission electron microscopy (HRTEM) was used to study the microstructure in more detail.

A HRTEM image of a typical Ni–BCTZ interface obtained from the 3 wt.% TiO_2-doped Ni internal electrode in MLCC is shown in Fig. 6. The thickness of the Ni electrode was approximately 2.5 μm, which is similarly in thickness to Ni observed from the SEM, as shown in Fig. 6(a). The interface between Ni electrodes and BCTZ dielectrics is clear, which may imply that no inter-reaction occurred at the interface. The sample shows the presence of many dislocations in the Ni electrode, as shown in Fig. 6(b) and (c). This phenomenon may be explained by lattice distortion, which arises from the substitution of Ni for Ti, creating lattice strain and nickel vacancies. These may be attributed to the ionic radius of Ni^{2+} (0.69 Å), which is larger than that of Ti^{4+} (0.605 Å).[27] When Ti substitutes into Ni sites in the FCC structure, it will create lattice strain and nickel vacancies. Dislocations are created during the solidification of crystalline solids and are also formed by the permanent or plastic deformation of crystalline solids, vacancy condensation and atomic mismatch in solid solutions.

Fig. 7 shows the microstructure of a BCTZ MLCC, and several small particles were observed in the Ni electrodes, as shown in Fig. 7(a). To confirm the existence of TiO_2 in Ni electrode after co-firing, Ti elemental mapping was performed for the MLCC specimens with the 3 wt.% TiO_2-doped Ni inner electrode, as shown in Fig. 7(b). The Ti signal is represented by the green points; thus, it was found that some Ti ions still existed in the Ni electrodes. That can also be proved by EDS analysis as shown in Fig. 7(c), EDS results, which show significant signal intensities in Ti. According to the X-ray diffraction analysis in the previous section, the TiO_2 phase was clearly shown to exist at $TiO_2 \geq 1$ wt.%. It is therefore believed that the small particles are composed of TiO_2.

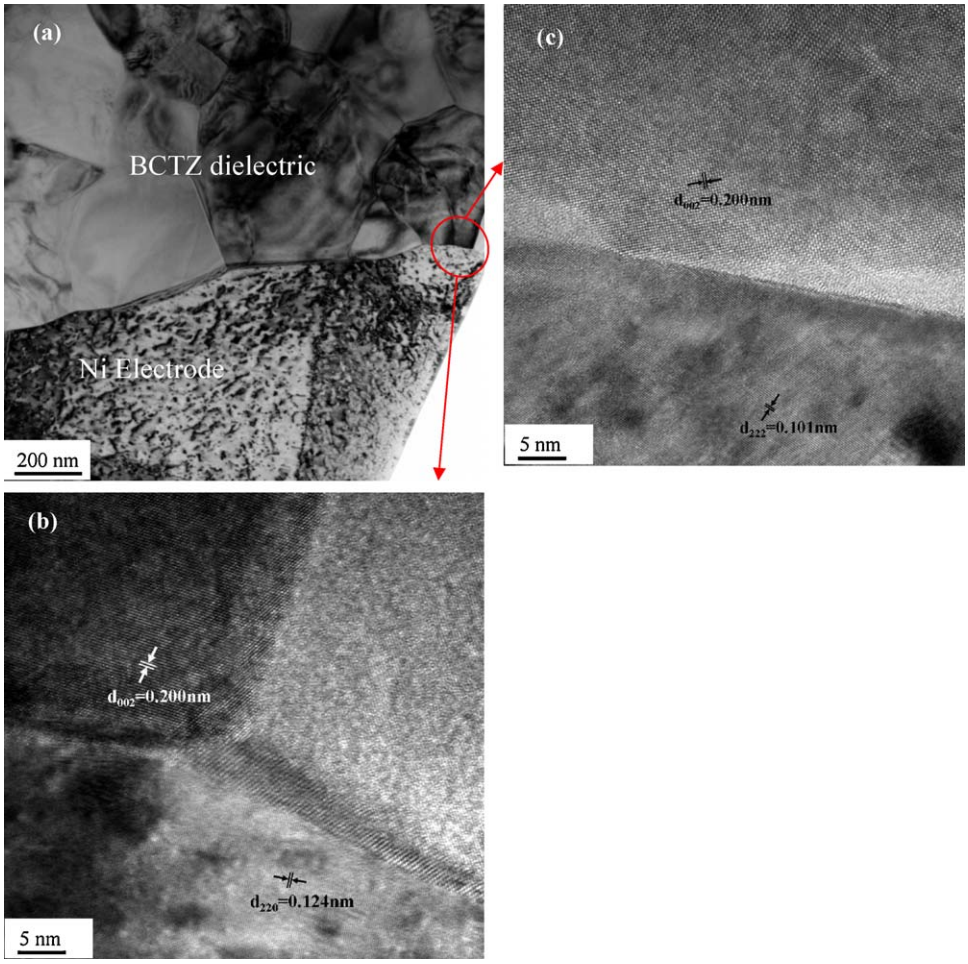

Fig. 9. HRTEM micrographs and selected-area diffraction patterns of a grain in BCTZ MLCC with 3 wt.% TiO_2-doped Ni electrodes sintered at 1220 °C (a), TEM micrographs (b) and (c) the interface between BCTZ and the electrode.

A HRTEM image of a typical Ni–BCTZ interface obtained from the 3 wt.% TiO_2-doped Ni internal electrode MLCC is shown in Fig. 8. The sample shows the presence of twins at the interface between BCTZ and the metal electrode, as can be seen in Fig. 8(a). This phenomenon can be explained by lattice distortion, which is the result of Ti diffusing into the BCTZ dielectrics, creating lattice strain. Twins are a two-dimensional defect. A twin is defined as a region in which a mirror image of the structure exists across a plane or a boundary. Unlike dislocation glide, movement of a twin boundary significantly and permanently alters the orientation of the crystal. The orientation of the twin plane and the misorientation across the twin boundary will be precisely the same for any particular type of twin.[28] The electron diffraction patterns of the BCTZ MLCC with the 3 wt.% TiO_2-doped Ni electrode in normal and twin grains were obtained and are shown in Fig. 8(b) and (c). Both the normal BCTZ grain (A) and twin BCTZ grain (B) were considered to be $BaTiO_3$ according to the electron diffraction patterns.

A HRTEM micrograph of BCTZ MLCC with the 3 wt.% TiO_2-doped Ni electrode sintered at 1220 °C were obtained and are shown in Fig. 9. It can be seen that there are no intermetallic layers at the interface between BCTZ and the metal electrode in the sample, as shown in Fig. 9(b) and (c). This can be inferred from the homogeneous image contrast in the Ni grain, which terminates at the interface. This indicates that no severe reduction of BCTZ occurred in the samples. Yang et al.[10] reported that such observations of the Ni–$BaTiO_3$ interface were performed on more than 20 commercial Ni–$BaTiO_3$ MLCCs supplied by a number of manufacturers. A discrete interface layer was present in all samples. The thickness of the interface layer ranged from 4 to 15 nm, most likely depending on the exact doping chemistry, binder chemistry in the Ni electrodes, $BaTiO_3$ powder sources, $BaTiO_3$ tapes, and process history of different manufacturers.

3.3. *Effect of TiO_2 doped Ni electrodes on the dielectric properties of BCTZ MLCC*

Fig. 10 shows the temperature coefficient of capacitance (TCC) as a function of the amount of TiO_2 dopant in the nickel paste. For samples with 0, 1, and 3 wt.% TiO_2 dopant, the Curie temperatures were 0 °C, 21.8 °C, and 30.2 °C, respectively. The Curie point shifted to a higher temperature when the TiO_2 dopant was added to Ni. The reason for this may be due to slight changes in the *A*/*B* ratio of BCTZ dielectrics when TiO_2-doped Ni electrodes were employed. On the other

Table 1
The dielectric constant and dielectric loss of the BCTZ MLCCs as a function of the TiO_2 dopants.

TiO_2 (wt.%)	Sintering temperature (°C)	Dielectric constant	Dielectric loss ($\times 10^{-4}$)	Resistance (MΩ)	Curie point (°C)
1	1220	20500	1080	1.1×10^5	21.8
3	1220	22100	1195	9.6×10^4	30.2

hand, the Curie point shifted to a higher temperature with a decreasing *A*/*B* ratio, resulting in higher permittivity at room temperature.

The dielectric constant and dielectric loss of the BCTZ ceramics as a function of the TiO_2 dopants and sintering temperatures were determined at 1 kHz, and the results are listed in Table 1. The ε_r value of the BCTZ MLCC without the addition of TiO_2 sintered at 1220 °C was very low (~10,000).[8] The dielectric constants of the BCTZ MLCC sintered at 1220 °C are 20,500 and 22,100 when doped with 1 and 3 wt.% TiO_2 in Ni paste, respectively. It is common that the dielectric constant is greater for the BCTZ MLCC sintered at 1220 °C with TiO_2 dopant than without the TiO_2 dopant. That can be attributed to the TCC shift (closer to room temperature) and good electrode continuity of the BCTZ MLCC with the TiO_2-doped Ni electrodes. Jain et al.[29] have reported that the permittivity at room temperature was found to increase with decreasing *A*/*B* ratios. Hansen et al.[30] mentioned that the broad dielectric maxima increased with increasing grain size. Moreover, Fig. 5(c) and (d) shows that the average grain size of the samples under the same sintering conditions increased with increasing TiO_2 content (decreasing *A*/*B* ratio). Thus, one of the factors for the increase in permittivity actually results from the growth of grains.

The loss tangent of the BCTZ MLCCs is also listed in Table 1. For samples with different TiO_2 dopant ranging from 1 to 3 wt.%, the dielectric loss of BCTZ MLCCs is higher than that of MLCCs containing Ni electrode without TiO_2 dopant. Additionally, the insulation resistance of the samples with different sintering temperatures and Ti dopants are listed in Table 1. The insulation resistance of all samples was approximately 1×10^{11} Ω, implying the whole samples were well densification.

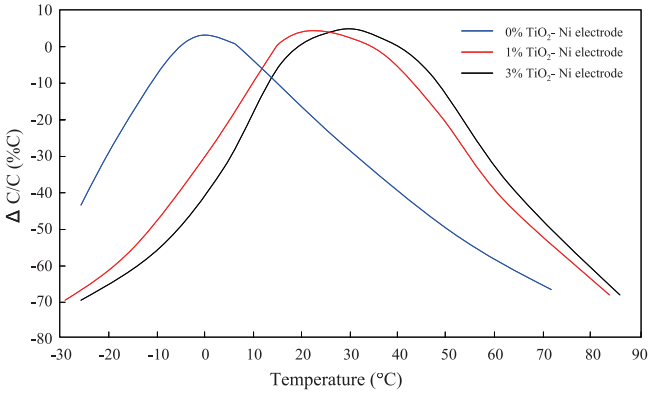

Fig. 10. Temperature coefficient of capacitance of BCTZ MLCCs sintered at 1220 °C as a function of the amount of added TiO_2 into the Ni electrode.

4. Conclusions

The shrinkage behaviour, microstructure development, and dielectric properties of BCTZ MLCC with TiO_2-doped Ni electrodes have been investigated. The TEM conclusions revealed that there was almost no interaction between the TiO_2-doped Ni electrodes and the BCTZ dielectric layer. Unlike commercial MLCCs, this result showed that the interface between TiO_2-doped Ni electrodes and the BCTZ dielectric layer was very clean. However, an intermetallic layer at the interface between the BT dielectric and the Ni electrode were observed in a commercial MLCC. The continuities of the MLCC electrodes were compared, and the continuities of the electrode for the conventional Ni electrode and TiO_2-doped Ni electrode were approximately 80% and 90%, respectively. The continuity of MLCC electrodes improved significantly with TiO_2-doped Ni electrodes due to no trigger mutual reaction between Ni and BCTZ. Moreover, the microstructures of BCTZ dielectrics were only slightly influenced by TiO_2 doping, as more TiO_2 dopant in the Ni electrode led to marginally increasing grain growth of the BCTZ dielectrics. This may be attributed to a slight change in the *A*/*B* ratio of BCTZ dielectrics during sintering. Additionally, BCTZ MLCCs with a TiO_2-doped Ni electrode had positive effects on the dielectric constant and electrode continuity.

References

1. Rae A, Chu M, Ganine V. Barium titanate past, present and future. In: *Ceramic Transactions, vol. 100, Dielectric Ceramic Materials '98.*; 1999. pp. 1–12.
2. Li T, Li LT, Kou Y, Gui ZL. Stable temperature dependence of dielectric properties in $BaTiO_3$–Nb_2O_5–Co_3O_4–Gd_2O_3 system. *J Mater Sci Lett* 2000;**19**:995–7.
3. Hansen P, Hennings DFK, Schreinemacher H. High-k dielectric ceramics from donor/acceptor co-doped (BaCa)(TiZr)O_3. *J Am Ceram Soc* 1998;**81**:1369–74.
4. Lee YC, Lu WH, Shieu FS. Investigation of thin film end-termination on multilayer ceramic capacitors with base-metal-electrode. *Ceram Int* 2009;**35**:869–74.
5. Shizuno H, Kusumi S, Saito H, Kishi H. Properties of Y5V multilayer ceramic capacitor with nickel electrodes. *Jpn J Appl Phys* 1993;**32**:4380–3.
6. Chen R, Wang X, Wen H, Li L, Gui. Z. Enhancement of dielectric properties by additions of Ni nano-particles to a X7R-type barium titanate ceramic matrix. *Ceram Int* 2004;**30**:1271–4.
7. Kishi H, Mizuno Y, Chazono H. Base-metal electrode-multilayer ceramic capacitors: past, present and future perspectives. *Jpn J Appl Phys* 2003;**42**:1–15.
8. Lee Y-C, Lin C-W, Chen W-J, Lu. W-H. The influence of SiO_2 addition on the dielectric properties and microstructure of $(Ba_{0.96}Ca_{0.04})(Ti_{0.85}Zr_{0.15})O_3$ ceramics sintered in reducing atmosphere. *Intl J Appl Ceram Technol* 2009;**6**:692–701.
9. Yamamatsu J, Kawano N, Arashi T, Sato A, Nakano Y, Nomura T. Reliability of multiplayer ceramic capacitors with nickel electrodes. *J Power Sources* 1996;**60**:199–203.

10. Yang GY, Lee SI, Liu ZJ, Anthony CJ, Dickey EC, Liu ZK, et al. Effect of local oxygen activity on Ni–$BaTiO_3$ interfacial reactions. *Acta Mater* 2006;**54**:3513–23.
11. Lee Y-C, Lee C-T, Lee W-H, Shieu F-S. A study of ceramics addition in end termination of cofired multilayer ceramic capacitors. *Mater Chem Phys* 2006;**100**:355–60.
12. Sakabe Y. Dielectric materials for base-metal multilayer ceramic capacitors. *Am Ceram Soc Bull* 1987;**66**:1338–41.
13. Halder N, Chattopadhyay D, Sharma AD, Saha D, Sen A, Maiti HS. Effect of sintering atmosphere on the dielectric properties of barium titanate based capacitors. *Mater Res Bull* 1991;**36**:905–13.
14. Kang J-H, Joo D, Cha H-M, Jung Y-G, Paik U. Shrinkage behavior and interfacial diffusion in Ni-based internal electrodes with $BaTiO_3$ additive. *Ceramics Int* 2008;**34**:1487–94.
15. Paik U, Kang KM, Jung YG, Kim J. Binder removal and microstructure with burnout condition in $BaTiO_3$ based Ni–MLCCs. *Ceram Int* 2003;**29**:939–46.
16. Park DH, Jung YG, Paik U. Crack suppression behavior with postprocess parameters in $BaTiO_3$ based Ni–MLCCs. *Ceram Int* 2005;**31**:655–61.
17. Bordia RK, Scherrer GW. On constrained sintering: I. Constitutive model for a sintering body. *Acta Metall* 1988;**36**:2393–7.
18. Chowdary KR, Subbarao EC. Liquid phase sintered $BaTiO_3$. *Ferroelectrics* 1981;**37**:689–92.
19. Burn I. Flux-sintered $BaTiO_3$ dielectrics. *J Mater Sci* 1982;**17**:1398–408.
20. Haussonne JM, Desgardin G, Bajolet PH, Raveau B. Barium titanate perovskite sintered with lithium fluoride. *J Am Ceram Soc* 1983;**66**:801–7.
21. Desgardin G, Mey I, Raveau B. $BaLiF_3$—a new sintering agent for $BaTiO_3$-based capacitors. *Am Ceram Soc Bull* 1985;**64**:563–70.
22. Virkar AN, Sundaram SK. Studies on the effect of minor glass additives on the sintering and dielectric properties of barium titanate. *Trans Indian Ceram Soc* 1985;**44**:71–4.
23. Sarkar SK, Sharma ML. Liquid phase sintering of $BaTiO_3$ by boric oxide (B_2O_3) and lead borate (PbB_2O_4) glasses and its effect on dielectric strength and dielectric constant. *Mater Res Bull* 2000;**24**:407–16.
24. Hanaor D, Sorrell C. Review of the anatase to rutile phase transformation. *J Mater Sci* 2011;**46**:855–74.
25. Jamieson J, Olinger B. Pressure temperature studies of anatase, brookite, rutile and TiO_2. II: A discussion. *Mineral Notes* 1969;**54**:1477–80.
26. Lee W-H, Tseng T-Y, Hennings D. Effects of A/B cation ratio on the microstructure and lifetime of $(Ba_{1-x}Ca_x)_z(Ti_{0.99-y}Zr_yMn_{0.01})O_3$ (BCTZM) sintered in reducing atmosphere. *J Mater Sci: Mater Electron* 2000;**11**:157–62.
27. Lee Y-C, Huang Y-L. Effects of CuO doping on microstructural and dielectric properties of the $Ba_{0.6}Sr_{0.4}TiO_3$ ceramics. *J Am Ceram Soc* 2009;**92**:2661–7.
28. Eibl O, Pongratz P, Skalicky P. Formation of (1 1 1) twins in $BaTiO_3$ ceramics. *J Am Ceram Soc* 1987;**70**:C195–7.
29. Jain TA, Fung KZ, Chan J. Effect of the A/B ratio on the microstructures and electrical properties of $(Ba_{0.95\pm x}Ca_{0.05})(Ti_{0.82}Zr_{0.18})O_3$ for multilayer ceramic capacitors with nickel electrodes. *J Alloys Compd* 2009;**468**:370–4.
30. Hansen P, Hennings D, Schreinemacher H. Dielectric properties of acceptor-doped (Ba,Ca)(Ti, Zr)O_3 ceramics. *J Electroceram* 1998;**2**:85–94.